CHEMISTRY
A EUROPEAN JOURNAL

DOI: 10.1002/chem.200600454

Formation of Disperse Nanoparticles at the Oil/Water Interface in Normal Microemulsions

Jian-Ping Ge, Wei Chen, Li-Ping Liu, and Ya-Dong Li*[a]

Abstract: An artificial oil/water interface was created in normal microemulsions. Various well-dispersed inorganic nanoparticles were successfully fabricated at this micelle interface, and a "hot liquid annealing" process was used to crystallize the products. Owing to the large solubility of the source materials in the water phase, the colloidal nanoparticles can easily be prepared on a large scale. Compared with traditional reverse-microemulsion methods, the method reported here yields larger amounts of colloidal particles but with the same quality.

Keywords: colloids · interfaces · microemulsions · nanocrystals

Introduction

The emergence of a new concept or method in science and technology always forces the advancement of the concerned subjects and accelerates the spread of related applications. Looking at the history of chemical synthesis, the discovery and development of sol–gel, hydrothermal, metalorganic chemical vapor deposition (MOCVD) techniques, and so forth, have provided an abundance of functional powders, glasses, films, and artificial crystals, which have greatly promoted scientific research and social manufacture. Things are the same for the recently arisen field of nanoscience, in which some important synthetic methods, such as the pyrolysis of organometallic compounds,[1–5] liquid–solid–solution (LSS) strategy,[6] vapor–liquid–solid (VLS) growth,[7–9] and reverse microemulsion,[10–15] were established to produce high-quality and size-tunable nanoparticles and nanowires, thus pushing the entire area of nano research to a higher level. It is interesting to find that all of these methods involve reactions occurring at an interface, such as organic/inorganic, vapor/liquid, liquid/solid, and water/oil interfaces. Inspired by the special interface activity, we designed an oil/water interface-controlled reaction in normal microemulsions (water/surfactant/hexane) to produce dispersive colloidal nanocrystals. Owing to the large solubility of the source materials in the water phase, the colloidal nanoparticles can easily be prepared on a large scale; this should yield considerably larger amounts compared with the traditional reverse-microemulsion method. According to the solubility product constant (K_{SP}) of each specific reaction, the crystallinity of the products is controllable, and "hot liquid annealing" was applied to make crystalline colloidal nanoparticles. It is believed that this general method will lead to a better understanding of the flexible manipulation of the interface

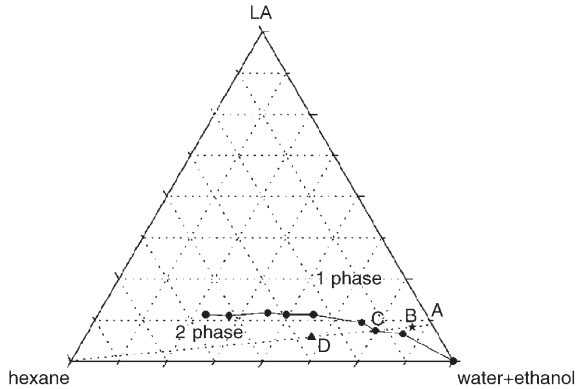

Figure 1. Empirical phase diagram of the H_2O/EtOH/NaLA/LA/hexane microemulsions. The composition is described using volume fractions. The water/ethanol ratio is always 1:1. The NaLA/LA molar ratio is always 2:3, and the total volume of LA is considered as the surfactant volume. The phase diagram is determined by gradual addition of hexane to a one-phase H_2O/EtOH/NaLA/LA mixture with a constant volume fraction. For instance, we start from point A, and reach a critical point C where the solution begins to exhibit a two-phase character.

[a] J.-P. Ge, W. Chen, L.-P. Liu, Prof. Y.-D. Li
Department of Chemistry
Tsinghua University
Beijing, 100084 (P.R. China)
Fax: (+86) 10-6278-8765
E-mail: ydli@mail.tsinghua.edu.cn

Supporting information for this article is available on the WWW under http://www.chemeurj.org/ or from the author.

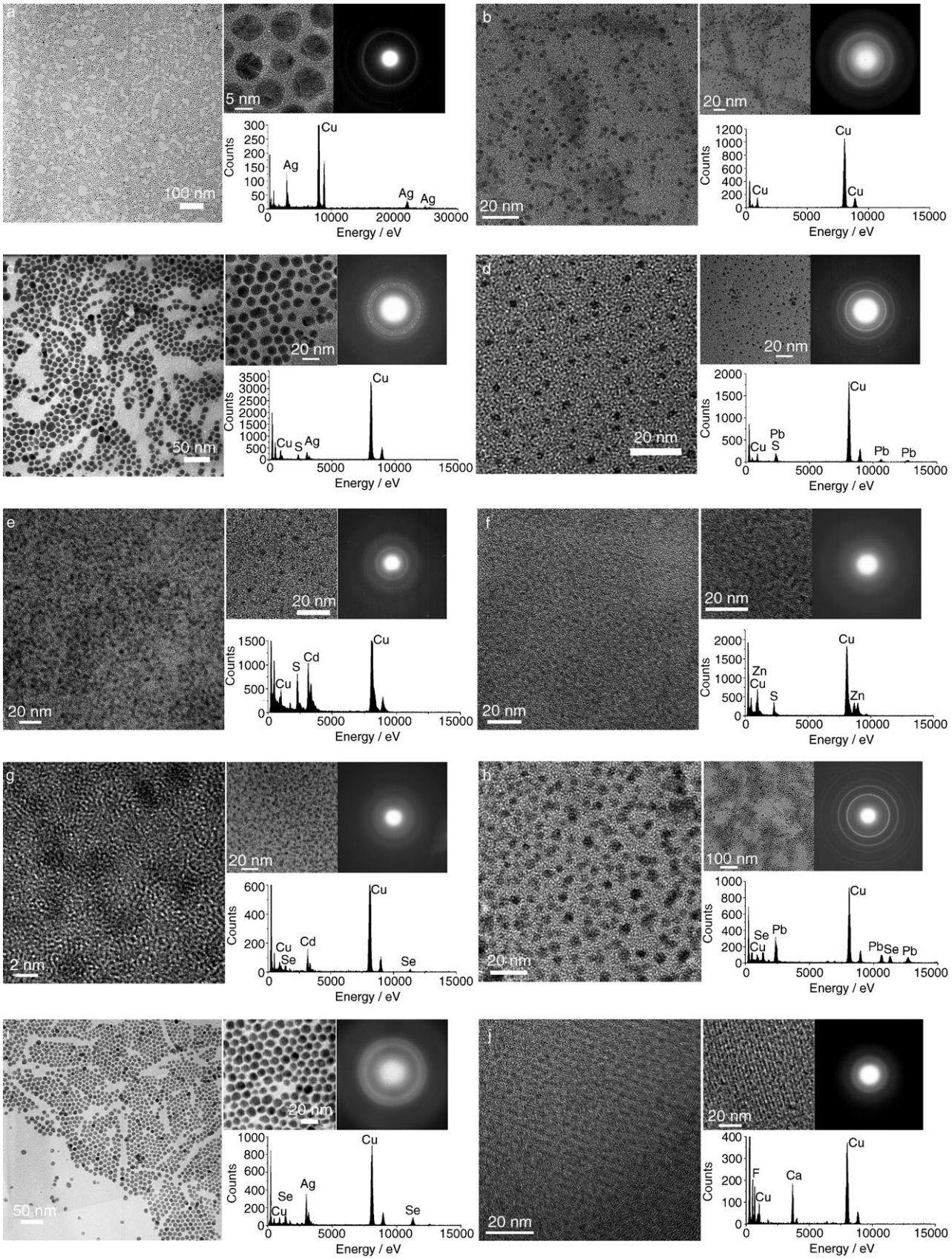

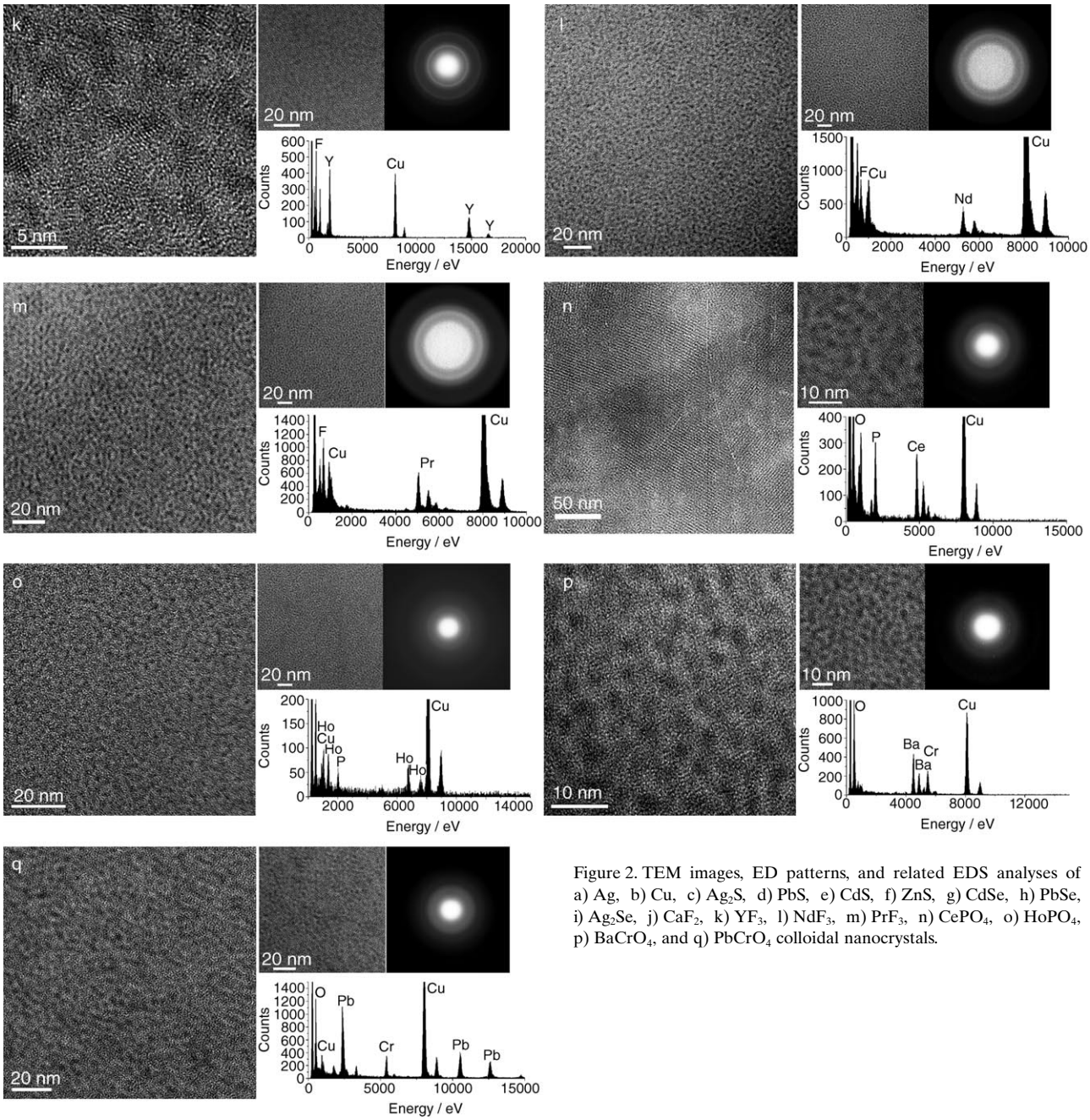

Figure 2. TEM images, ED patterns, and related EDS analyses of a) Ag, b) Cu, c) Ag_2S, d) PbS, e) CdS, f) ZnS, g) CdSe, h) PbSe, i) Ag_2Se, j) CaF_2, k) YF_3, l) NdF_3, m) PrF_3, n) $CePO_4$, o) $HoPO_4$, p) $BaCrO_4$, and q) $PbCrO_4$ colloidal nanocrystals.

in the multiphase system, and it will be advantageous in supplying a large amount of product for current magnetic,[16–18] optical,[19–22] catalytic,[23–28] battery,[29,30] and biological[31,32] applications.

Results and Discussion

Firstly, the phase behavior of the system was studied to obtain the appropriate microemulsions. Figure 1 shows the empirical phase diagram for the water/ethanol/sodium linoleate (NaLA)/linoleic acid (LA)/hexane mixtures at room temperature (293 K). NaLA, LA, and EtOH were used to stabilize this oil-in-water microemulsion. Because of the complexity of the five-component system, the phase diagram was simplified to an empirical ternary phase diagram, which is composed of total LA (including the part to generate NaLA with NaOH), water plus ethanol, and hexane.

The one-phase/two-phase envelope extends from the point of pure H_2O+EtOH to the point at 28.17% H_2O+EtOH, 57.75% hexane, and 14.08% LA, and the two-phase part is located in the lower LA region. According to the phase diagram measurement, it can be concluded that with an increase of the ratio of LA/(H_2O+EtOH), more hexane

can be dissolved into their mixtures to form a thermostable system. Because we were focusing on the oil-in-water microemulsion, more attention was paid to the right-bottom region. The actual point we used is marked (point B) in the phase diagram, and is located in the normal microemulsion region.

Typical transmission electron microscopy (TEM) pictures, electron diffraction (ED) patterns, and energy dispersive spectroscopy (EDS) results are presented in Figure 2. Only the peaks representing the elements of the expected products and Cu, C, and O environmental impurities are found in each EDS spectrum, indicating that the colloidal particles are highly pure. All the products are made up of small particles with average sizes of 2 to 13 nm and were well spread over the copper-grid-supported carbon films. Generally, high-energy electron irradiation at large magnifications causes the evaporation and decomposition of the organic solvent and surfactant, which leads to some slight aggregation. This phenomenon is especially common in the case of amorphous particles.

From the TEM observations, all the colloidal particles can be classified as crystalline or amorphous, which is foreseeable chiefly according to the change in the Gibbs free energy (ΔG) of each reaction. Small ΔG values (or small K_{SP} of the precipitate) lead to crystalline products, such as Ag, Cu, Ag_2Se, Ag_2S, PbS, and PbSe particles. They all have regular spherical shapes and clear electron-diffraction rings. Electron beam irradiation had little effect on the TEM observation. On the contrary, relatively large ΔG (or K_{SP}) values result in particles with poor crystallinity or amorphous characteristics. The small particles commonly have irregular shapes and pale ED patterns. Irradiating the samples with an electron beam over a longer period of time further increased the irregularity of the morphologies. Of course, the actual system is much more complicated than that described here and other factors will also affect the crystallinity, such as the coordination strength between the metals and surfactants.

In addition to the difference in TEM analyses, these two types of nanoparticle are also distinguished by their XRD patterns. Figure 3 shows the XRD patterns of all of the powders that were produced as precipitates from hexane by adding enough ethanol. The patterns of the crystalline particles have characteristic peaks that match well with the JCPDS cards. The others patterns consist of two to three broad peaks shielding a group of separate peaks, which shows that the products are amorphous. Regardless of the kind of peak present in the pattern, all the peaks are seriously broadened, indicating that the particles are fairly small according to the Debye–Scherrer formula.

Because the amorphous characteristics of the products discussed in this paper may limit their application, a "hot liquid annealing" technique was used to effectively solve this problem. We shall describe the treatment of $BaCrO_4$ as a typical example (for consistency, this will also be used as the example in the Experimental Section). Before the post-treatment, the microemulsion was transferred to a stainless

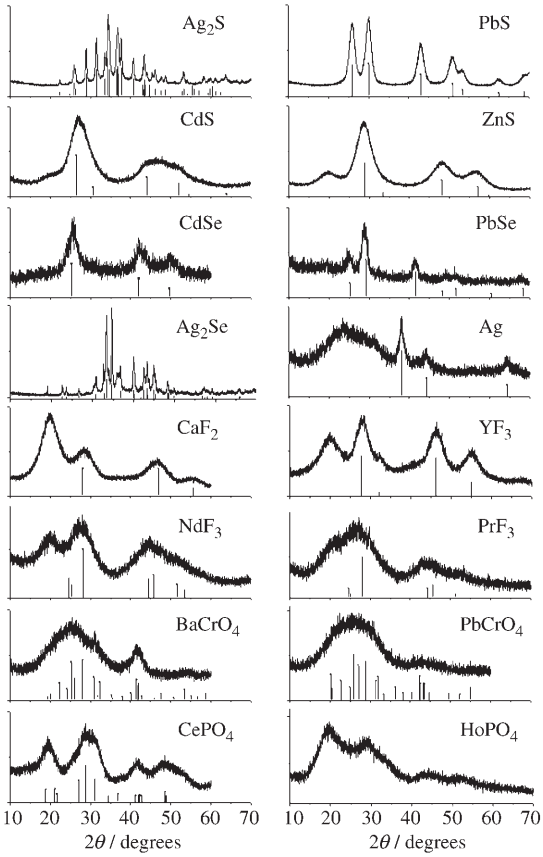

Figure 3. XRD patterns for the sulfide, selenide, metal, fluoride, phosphate, and chromate nanoparticles.

steel Teflon-lined autoclave and heated at 140 °C for 24 h. The sealed autoclave provides a high-temperature environment for the annealing of $BaCrO_4$ amorphous nanoparticles for which you do not need to worry about the evaporation of the solvent. After 24 h of aging, the autoclave was cooled down to room temperature and the samples deposited at the bottom were washed with ethanol and re-dispersed in hexane. TEM images and ED patterns of the products are shown in Figure 4, which proves that the amorphous irregular particles have been gradually assembled into short crystalline $BaCrO_4$ nanorods. When ethanol was substituted with methanol, spherical crystalline $BaCrO_4$ nanoparticles formed instead.

From the results above, the developed method was confirmed to be a successful manipulation of the interface in the oil/water system, and a mechanism based on the "interface-controlled reaction" was proposed to describe the formation of all of the nanoparticles (Figure 5) as follows: First, the transparent oil-in-water normal microemulsion forms after all the components are added according to the designed volume ratio. When metal cations such as Ba^{2+} were added to the solution, they were absorbed around the oil core due to the Coulomb attraction between Ba^{2+} and LA^-. Because the ions also have strong solvation properties in polar solvents, they will prefer to stay at the oil/water (O/

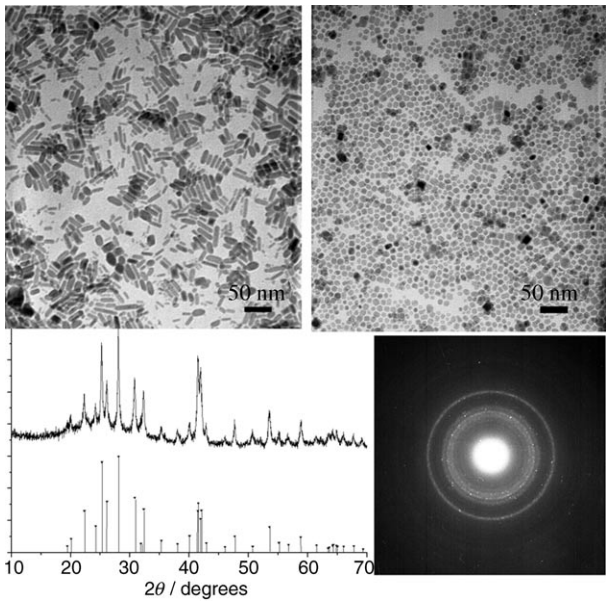

Figure 4. TEM, XRD, and ED analyses of crystallized $BaCrO_4$ nanorods and nanoparticles produced by hot liquid annealing in ethanol- and methanol-composed microemulsions, respectively (XRD and ED results are for the nanorods).

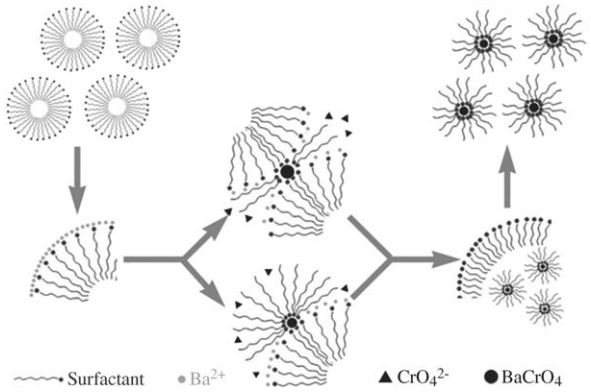

Figure 5. Proposed mechanism for the synthesis of colloidal nanoparticles with the interfacial manipulations in normal micelles.

W) interface, so that they are stabilized by both the polar solvent and the surfactant molecules. However, the injection of anions such as CrO_4^{2-} will destroy this balance by the "interface reaction" with Ba^{2+}. Considering the low solubility of these inorganic compounds, the original cations will quickly combine with the anions to produce small particles at the O/W interface. As the major phase in a normal microemulsion is water and ethanol, the whole process will be as fast as that in the common aqueous solutions. Actually, the precipitation occurs within seconds in most cases. The interface reaction may occur through two pathways. One is that the anions react with the cations located in the region close to a single micelle interface. The other may occur through the random collisions of two micelles, in which case the anions react with the cations from both interfaces. But regardless of the path it takes, the formed particles have a neutral electric charge, which makes them unable to be as stable as the original cations at the interface. Because the particles were capped with surfactant, it is reasonable to predict a "phase transfer", that is, that the particles move from the O/W interface to the inner oil core. Following this, the normal micelles recover owing to the supply of certain surfactant molecules free in the water phase, making them prepared for the next "interface reaction". The dynamic "reaction transfer" process happens alternatively and frequently, inducing the production of nanoparticles in a large amount and at a fast rate. Finally, hexane was added to destroy the single-phase status of the system, which is illustrated in the phase diagram (Figure 1, point B to point D). The products extracted from the upper organic phase were washed with ethanol and re-dispersed in a nonpolar solvent.

The difference between this normal microemulsion and the traditional reverse microemulsion lies in the microscale mechanisms. Generally, in a typical reverse microemulsion, the small size of the micelles subjects them to continuous Brownian motion. Collisions between micelles will lead to the formation of a short-lived ($\approx$100 ns) dimer. When two reverse micelles composed of cation A and anion B are mixed together, they will exchange the content of the aqueous cores through the dimers, resulting in the eventual equilibrium distribution of all content. Then the reactions are performed inside the micelle cores, and particles will have nearly uniform size and shape due to the confinement of micelles.[33,34] In our normal microemulsion process, reactions were taking place at the interface of the normal micelles. Because of the polarity inverse caused by the neutralization, the particles were transferred to the oil phase. In the hot liquid annealing process, the amorphous particles in the oil core reorganized and crystallized to give larger particles due to Ostwald ripening. The shape and size may also be controlled by the confinement of micelles, which is similar to the situation in reverse microemulsions.

Conclusion

In conclusion, an interface-controlled reaction in a normal microemulsion was designed to fabricate various inorganic nanoparticles that are small and have good dispersibility in nonpolar organic solvents. This method has its natural merit in yielding nanoparticles in a large amount and with high productivity. A "hot liquid annealing" process was used to make crystalline products, which provide abundant nanomaterials for catalytic, photoelectric, and biological applications.

Experimental Section

Materials: All the reagents used in this work, including NaOH, linoleic acid (LA, $C_{17}H_{31}COOH$), C_2H_5OH, *n*-hexane, and the various source reactants listed in Table 1 were of A.R. grade from the Beijing Chemical

Table 1. Summary of the source materials, K_{SP}, size, and crystallinity for all products.

Compound	Source materials		K_{SP}	Size [nm]	Crystallinity
CdS	$Cd(NO_3)_2$[a]	Na_2S[a]	8.0×10^{-27}	2.0–4.0	poorly crystalline
ZnS	$Zn(NO_3)_2$[a]	Na_2S[a]	2.5×10^{-22}	2.5–4.5	poorly crystalline
Ag_2S	$AgNO_3$[b]	Na_2S[a]	6.3×10^{-50}	9.0–13.0	crystalline
PbS	$PbAc_2$[a]	Na_2S[a]	1.3×10^{-28}	2.5–3.0	crystalline
CdSe	$Cd(NO_3)_2$[a]	Na_2SeSO_3[a]	6.3×10^{-36}	2.0–3.0	poorly crystalline
Ag_2Se	$AgNO_3$[b]	Na_2SeSO_3[a]	2.0×10^{-64}	8.0–10.0	crystalline
PbSe	$PbAc_2$[a]	Na_2SeSO_3[a]	7.9×10^{-43}	4.0–6.0	crystalline
CaF_2	$CaCl_2$[a]	NaF[b]	2.7×10^{-11}	2.0–3.0	amorphous
YF_3	$Y(NO_3)_3$[a]	NaF[c]	6.6×10^{-13}	3.0–4.0	amorphous
PrF_3	$Pr(NO_3)_3$[a]	NaF[c]	7.1×10^{-17}	1.5–2.5	amorphous
NdF_3	$Nd(NO_3)_3$[a]	NaF[c]	–	1.5–2.0	amorphous
$HoPO_4$	$Ho(NO_3)_3$[a]	NaH_2PO_4[b]	–	2.0–3.0	amorphous
$CePO_4$	$Ce(NO_3)_3$[a]	NaH_2PO_4[b]	–	3.0–5.0	amorphous
$PbCrO_4$	$PbAc_2$[a]	K_2CrO_4[a]	2.8×10^{-13}	3.0–4.0	amorphous
$BaCrO_4$	$Ba(NO_3)_2$[a]	K_2CrO_4[a]	1.2×10^{-10}	2.0–4.0	amorphous
Ag	$AgNO_3$[a]	N_2H_4[d]	–	6.0–8.0	crystalline
Cu	$CuSO_4$[a]	N_2H_4[e]	–	2.0–3.0	crystalline

[a] 0.5 mmol. [b] 1.0 mmol. [c] 1.5 mmol. [d] 80%; 1.0 mL. [e] 80%; 3 mL.

Factory, China. The Na_2SeSO_3 solution used as the selenium source was prepared by placing selenium powder (5 mmol) and Na_2SO_3 (5 mmol) in distilled water (50 mL) under reflux for 1 h.

Synthesis: A designed microemulsion was used to fabricate various colloidal nanoparticles, such as sulfides, selenides, metals, fluorides, phosphates, and chromates. As an example of a typical process, the synthesis of $BaCrO_4$ nanoparticles is described.

$BaCrO_4$ nanoparticles: NaOH (200 mg) was dissolved in a mixture of water (10 mL) and ethanol (15 mL), followed by the addition of linoleic acid (3.7 mL) and hexane (2 mL); this formed a transparent solution. Then, two separate aqueous solutions (2.5 mL) of $Ba(NO_3)_2$ (0.5 mmol) and K_2CrO_4 (0.5 mmol) were added to the above microemulsion one after the other, under vigorous stirring, to generate a bright yellow transparent solution.

A post-treatment based on extraction (see Figure 1 in the Supporting Information) was adopted to ensure the required rate of production. After several minutes of reaction time, hexane (15 mL) was added to destroy the one-phase solution. According to the phase diagram, the system moves from point B to point D, which is located at the two-phase region. This two-phase mixture gradually forms a clear boundary, above which should be the hexane region and part of the ethanol region. At the same time, the hydrophobic colloidal $BaCrO_4$ nanoparticles are also extracted into the upper layer. With precipitation by additional ethanol, and high-speed centrifugation, the products were re-dispersed in hexane to bring out a concentrated solution of $BaCrO_4$ in hexane (0.1 mol L^{-1}). This general manipulation is also effective for many other inorganic compounds. The corresponding experimental parameters are summarized in Table 1, and photographs of the products, which all present high stability and good dispersibility, are shown in Figure 2 of the Supporting Information.

Characterization: The samples were characterized by using a Bruker D8 Advance X-ray diffractometer (XRD) with $Cu_{K\alpha}$ radiation ($\lambda=$ 1.5418 Å). The size and morphology of the nanoparticles were obtained by using a JEOL JEM-1200EX transmission electron microscope and a Tacnai TF20 high-resolution transmission electron microscope. The EDS data were also obtained by using the high-resolution microscope.

Acknowledgement

This work was supported by NSFC 90406003 and the State Key Project of Fundamental Research for Nanomaterials and Nanostructures (2003CB716901).

[1] J. G. Brennan, T. Siegrist, P. J. Carroll, S. M. Stuczynski, L. E. Brus, M. L. Steigerwald, *J. Am. Chem. Soc.* **1989**, *111*, 4141.
[2] C. B. Murray, D. J. Norris, M. G. Bawendi, *J. Am. Chem. Soc.* **1993**, *115*, 8706.
[3] A. P. Alivisatos, *Science* **1996**, *271*, 933.
[4] X. G. Peng, L. Manna, W. D. Yang, J. Wickham, E. Scher, A. Kadavanich, A. P. Alivisatos, *Nature* **2000**, *404*, 59.
[5] Y. Yin, A. P. Alivisatos, *Nature* **2005**, *437*, 664.
[6] X. Wang, J. Zhuang, Q. Peng, Y. D. Li, *Nature* **2005**, *437*, 121.
[7] M. H. Huang, S. Mao, H. Feick, H. Q. Yan, Y. Y. Wu, H. Kind, E. Weber, R. Russo, P. D. Yang, *Science* **2001**, *292*, 1897.
[8] X. F. Duan, C. M. Lieber, *Adv. Mater.* **2000**, *12*, 298.
[9] A. M. Morales, C. M. Lieber, *Science* **1998**, *279*, 208.
[10] M. P. Pileni, *Langmuir* **1997**, *13*, 3266.
[11] M. Li, H. Schnablegger, S. Mann, *Nature* **1999**, *402*, 393.
[12] J. Eastoe, B. Warne, *Curr. Opin. Colloid Interface Sci.* **1996**, *1*, 800.
[13] H. Ohde, F. Hunt, C. M. Wai, *Chem. Mater.* **2001**, *13*, 4130.
[14] L. M. Qi, J. M. Ma, H. M. Cheng, Z. G. Zhao, *J. Phys. Chem. B* **1997**, *101*, 3460.
[15] S. Xu, H. C. Zhou, J. Xu, Y. D. Li, *Langmuir* **2002**, *18*, 10503.
[16] C. Liu, B. S. Zou, A. J. Rondinone, Z. J. Zhang, *J. Phys. Chem. B* **2000**, *104*, 1141.
[17] C. R. Vestal, Z. J. Zhang, *Chem. Mater.* **2002**, *14*, 3817.
[18] P. Tartaj, C. J. Serna, *J. Am. Chem. Soc.* **2003**, *125*, 15754.
[19] J. Jang, J. H. Oh, *Adv. Mater.* **2003**, *15*, 977.
[20] Z. Q. Ye, M. Q. Tan, G. L. Wang, J. L. Yuan, *Anal. Chem.* **2004**, *76*, 513.
[21] S. T. Selvan, T. T. Tan, J. Y. Ying, *Adv. Mater.* **2005**, *17*, 1620.
[22] Y. H. Yang, M. Y. Gao, *Adv. Mater.* **2005**, *17*, 2354.
[23] A. J. Zarur, J. Y. Ying, *Nature* **2000**, *403*, 65.
[24] M. Andersson, L. Osterlund, S. Ljungstrom, A. Palmqvist, *J. Phys. Chem. B* **2002**, *106*, 10674.
[25] Z. L. Liu, J. Y. Lee, M. Han, W. X. Chen, L. M. Gan, *J. Mater. Chem.* **2002**, *12*, 2453.
[26] J. C. Yu, L. Wu, J. Lin, P. S. Li, Q. Li, *Chem. Commun.* **2003**, 1552.

[27] D. Gao, R. R. He, C. Carraro, R. T. Howe, P. D. Yang, R. Maboudian, *J. Am. Chem. Soc.* **2005**, *127*, 4574.
[28] K. E. Price, D. T. McQuade, *Chem. Commun.* **2005**, 1714.
[29] C. H. Lu, H. C. Wang, *J. Mater. Chem.* **2003**, *13*, 428.
[30] K. Y. Chan, J. Ding, J. W. Ren, S. A. Cheng, K. Y. Tsang, *J. Mater. Chem.* **2004**, *14*, 505.
[31] S. Santra, P. Zhang, K. M. Wang, R. Tapec, W. H. Tan, *Anal. Chem.* **2001**, *73*, 4988.
[32] X. J. Zhao, R. Tapec-Dytioco, W. H. Tan, *J. Am. Chem. Soc.* **2003**, *125*, 11474.
[33] C. Burda, X. B. Chen, R. Narayanan, M. A. El-Sayed, *Chem. Rev.* **2005**, *105*, 1025.
[34] B. L. Cushing, V. L. Kolesnichenko, C. J. O'Connor, *Chem. Rev.* **2004**, *104*, 3893.

Received: April 1, 2006
Published online: June 14, 2006

